THE ASTROPHYSICAL JOURNAL, 277:791–805, 1984 February 15

EVOLUTION OF 8–10 $M_\odot$ STARS TOWARD ELECTRON CAPTURE SUPERNOVAE. I. FORMATION OF ELECTRON-DEGENERATE O + Ne + Mg CORES

KEN'ICHI NOMOTO[1]
Laboratory for Astronomy and Solar Physics, NASA Goddard Space Flight Center
Received 1983 March 4; accepted 1983 July 12

ABSTRACT

Helium cores in stars with masses near 10 $M_\odot$ are evolved from the helium burning phase; the outer edge of the core is fitted to the boundary conditions at the bottom of the hydrogen-rich envelope. Two cases with initial helium core mass of $M_H^{(0)} = 2.6\ M_\odot$ (case 2.6) and 2.4 $M_\odot$ (case 2.4) are studied. Both cores spend the carbon burning phase under nondegenerate condition and leave O + Ne + Mg cores. Further evolution depends on the mass of the O + Ne + Mg core, M_C.

For case 2.6, M_C exceeds a critical mass for neon ignition (1.37 $M_\odot$) so that a strong off-center neon flash is ignited. The neon and oxygen flashing layer moves inward.

For case 2.4, on the other hand, neon is not ignited because M_C is smaller than 1.37 $M_\odot$. Then the O + Ne + Mg core becomes strongly degenerate and a dredge-up of a helium layer by the penetrating surface convection zone starts. Further evolution up through the core collapse which is triggered by electron captures on ^{24}Mg and ^{20}Ne must be common to cases with $M_H^{(0)} = 2.0$–$2.5\ M_\odot$ (i.e., stellar mass of 8–10 $M_\odot$).

Therefore 8–10 $M_\odot$ stars would give rise to Type II supernova explosions which leave neutron stars behind. However, these stars would not contribute much to the nucleosynthesis in the Galaxy since the mass interior to the helium-burning shell is close to 1.4 $M_\odot$. Possible formation of hydrogen-deficient carbon stars and of O + Ne + Mg white dwarfs both in single stars and in close binary systems are discussed.

Subject headings: stars: evolution — stars: interiors — stars: supernovae — stars: white dwarfs — nucleosynthesis

I. INTRODUCTION

The study of presupernova evolution and supernova models of single stars, following pioneering papers by Hoyle and Fowler (1960) and Colgate and White (1966), has shown that there exist two major types of supernova explosion (see Sugimoto and Nomoto 1980; Wheeler 1981; Trimble 1982; Rees and Stoneham 1982; Nomoto 1982*d* for reviews): stars more massive than 10 $M_\odot$ evolve to develop iron cores which collapse to leave neutron stars or black holes behind, and stars of 6(±2)–8(±1) $M_\odot$ form electron-degenerate carbon-oxygen (C + O) cores and explode as a carbon deflagration supernova leaving no neutron star remnant.

Besides these two major types, another triggering mechanism for supernovae has been suggested, i.e., collapse of a degenerate core due to electron captures (Rakavy, Shaviv, and Zinamon 1967; Finzi and Wolf 1967). Until recently, however, only a little attention has been paid to this type of supernova; many people have imagined that stars which burn carbon nonexplosively could evolve up to the formation of the iron core. This might be due to the lack of detailed calculations of the presupernova evolution of 8(±1)–10(±1) $M_\odot$ beyond carbon burning. Only preliminary results were reported by Barkat, Reiss, and Rakavy (1974) who showed that their 8 $M_\odot$ star develops a degenerate core after nonexplosive carbon burning.

Following their suggestion, Miyaji *et al.* (1980) did a hydrodynamical calculation evolving a degenerate O + Ne + Mg core and found that electron captures on ^{24}Mg and ^{20}Ne trigger the collapse of the core prior to the initiation of explosive oxygen burning. Although the oxygen flash is ignited during the collapse, electron captures are rapid enough to overcome the oxygen deflagration so that the core continues to collapse up to neutron star density. This type of supernova is called an "electron capture supernova" and would be observed as a Type II supernova.

This result suggested the importance of exploring the evolution of stars which form degenerate O + Ne + Mg cores after carbon burning and to determine the exact mass range of these stars.

Recently, detailed evolutionary calculations for stars of masses around ~10 $M_\odot$ have begun (Nomoto 1980*a*, 1981; Nomoto *et al.* 1982; Woosley, Weaver, and Taam 1980; Weaver, Axelrod, and Woosley 1980). Preliminary results of these calculations have revealed that the evolution of 8–12 $M_\odot$ (in particular 8–10 $M_\odot$) stars is worth investigating in detail in view of the following points:

1. The evolution of 8–12 $M_\odot$ stars is quite sensitive to the stellar mass because this mass range is a transition region from electron-degenerate to nondegenerate stellar cores. Therefore, various types of supernova explosion are expected to occur in these stars.

2. Through the study of this mass range, we can determine the lowest mass of stars which give rise to Type II supernova explosion and produce neutron stars. This is important for comparison with statistics of supernovae and pulsars (e.g., Tammann 1982; Lyne 1982).

[1] On leave from Department of Physics, Ibaraki University, Japan.

3. Hydrodynamical behavior of the core collapse in 8–10 $M_\odot$ stars may be significantly different from that for more massive stars because a shock which forms at the core bounce has been shown to propagate more energetically for the smaller mass core (Hillebrandt 1982*a*, *b*; Arnett 1982).

4. The 8–10 $M_\odot$ stars are suggested to be the Crab nebula's progenitor in view of elemental abundances in the ejecta (Davidson *et al.* 1982; Nomoto 1982*c*; Nomoto *et al.* 1982; Woosley, Weaver, and Taam 1980; Hillebrandt 1982*b*).

5. The 8–10 $M_\odot$ stars are possible progenitors of O + Ne + Mg white dwarfs in close binary systems (Nomoto *et al.* 1979; Nomoto 1980*a*, 1981). These white dwarfs, if enough mass is accreted, are likely to collapse to form neutron stars.

In the present series of papers, I shall give the details of the calculations of the evolution of 8–10 $M_\odot$ stars as mentioned above (Nomoto 1981, 1983). I have evolved helium cores starting from central helium burning for three cases (2.6, 2.4, and 2.2) which correspond to the initial helium core mass of $M_{\rm H}^{(0)} = 2.6$, 2.4, and 2.2 $M_\odot$, respectively. These cores are supposed to be formed in stars of total masses of $M \approx 8.5$–11 $M_\odot$ with an approximate relation of $M \approx 4M_{\rm H}^{(0)}$ although the exact core mass–total mass relation depends on the composition (Becker and Iben 1979). In this paper (Paper I), I report the evolution of cases 2.6 and 2.4 through the ignition of an off-center neon flash (case 2.6) and the formation of a degenerate O + Ne + Mg core (case 2.4). Case 2.2 has been evolved even further, from the dredge-up of a helium layer through the collapse triggered by electron captures on ^{24}Mg and ^{20}Ne, which will be reported in Nomoto (1984, hereafter Paper II) (see Nomoto *et al.* 1982; Nomoto 1983). It is concluded that the mass range for electron capture supernovae is $8(\pm 1)$–$10(\pm 1)$ $M_\odot$.

In the next section, the method of computation and input physics are given. In § III, the gravitational contraction of hypothetical pure neon stars is discussed in order to clarify the effect of electron degeneracy on neon ignition and stellar evolution, which is crucial for 8–10 $M_\odot$ stars. In § IV, the evolution from helium burning through the phase of the developing O + Ne + Mg core is summarized. Neon ignition for case 2.6 is described in § V, and the formation of a strong degenerate core for case 2.4 is discussed in § VI. In § VII, the composition structure at the end of the calculation is shown. Further evolution toward supernova stages, possible formation of O + Ne + Mg white dwarfs, and the origin of hydrogen-deficient carbon stars are discussed in § VIII. In § IX, a summary is given.

II. METHOD OF CALCULATION AND INPUT PHYSICS

a) *Models*

In the advanced phase of stellar evolution, the star is separated into two parts, i.e., the hydrogen-exhausted core and the hydrogen-rich envelope. The density gradient at the hydrogen-burning shell is so steep that the outer edge of the core can be regarded as a *quasi surface* of the core. Accordingly, the core evolves almost independently of the envelope (e.g., Hayashi, Hoshi, and Sugimoto 1962). For example, the core mass-luminosity relation for 3–8 $M_\odot$ stars does not depend on the total mass of the star (Paczyński 1970). In view of these characteristics of the evolved stars, the evolution is calculated in the following way.

The star is divided into the core and the hydrogen-rich envelope at the hydrogen-burning shell, where the hydrogen concentration is assumed to change discontinuously. The outer edge of the core and the bottom of the envelope are denoted by subscripts $1i$ and $1e$, respectively. When a quantity is continuous across the core-envelope interface, i or e will be omitted.

A Henyey-type calculation is carried out for the evolution of the core. The starting model is in the core helium burning stage with a composition of $Y = 0.98$ and $Z = 0.02$, where Y and Z denote the concentration of helium and heavier elements, respectively. Two cases for the initial core mass were chosen, i.e., $M_{\rm H}^{(0)} = 2.6\ M_\odot$ (case 2.6), and $2.4\ M_\odot$ (case 2.4). Total masses of stars for these cores were assumed to be $M = 4M_{\rm H}^{(0)}$ and the corresponding static hydrogen-rich envelopes with hydrogen concentration of $X = 0.602$, and $Z = 0.02$ were integrated (Nomoto and Sugimoto 1972) to be fitted to the outer edge of the core.

When the surface convection zone is not deep enough to reach the core-envelope interface, the envelope is replaced with the boundary conditions at the outer edge of the core. These conditions are obtained from the centrally condensed type of envelope solution (Chandrasekhar 1939) and are expressed as:

$$(2U + V - 4)_{1e} = 0\,, \tag{1}$$

$$L_{r,1e} = L_{\rm H} + L_{r,1i}\,, \tag{2}$$

where

$$\left(\frac{d\ln P}{d\ln T}\right)_{1e} = \frac{16\pi acGT^4M_r}{3P\kappa L_{r,1e}} = 4\,, \tag{3}$$

$$U \equiv \frac{d\ln M_r}{d\ln r} = \frac{4\pi r^3\rho}{M_r}\,, \tag{4}$$

$$V \equiv -\frac{d\ln P}{d\ln r} = \frac{GM_r\rho}{rP}\,. \tag{5}$$

Here, the symbols have their usual meanings (Sugimoto and Nomoto 1980, Appendix). The luminosity of the hydrogen shell burning, $L_{\rm H}$, is calculated by using a thin-shell approximation (Hayashi, Hoshi, and Sugimoto 1962) and $L_{r,1i}$ is the flux coming from the core. Thus the core mass is allowed to increase when the hydrogen shell burning processes the envelope material into helium. These boundary conditions, which do not depend on the stellar mass, have been found to be accurate enough by integrating static hydrogen-rich envelope (Nomoto and Sugimoto 1972; Nomoto 1974) and their validity was discussed in detail by Sugimoto and Nomoto (1980, p. 165). In fact the core mass-luminosity relation for 3–8 $M_\odot$ star is reproduced well by applying these conditions (Sugimoto and Nomoto 1975).

When the helium layer expands to induce penetration by the surface convection zone into the core, an actual core-envelope fitting is done and the core mass is allowed to decrease during the dredge-up of the helium layer.

b) *Input Physics*

The Henyey-type calculational method including both thermal and hydrodynamical equations (Sugimoto, Nomoto,

and Eriguchi 1981) and the input physics are mostly the same as used by Nomoto (1982*a*, *b*) except for the following.

Nucleosynthesis during helium, oxygen, and neon burning is treated as described by Arnett (1972*a*, 1974*a*, *b*). For carbon burning, the treatment by Endal (1975*b*) is modified to include ^{23}Na with a steady state abundance (A. S. Endal 1979, private communication). The neutrino processes included are photo, pair, and plasmon neutrino emission (Beaudet, Petrosian, and Salpeter 1967) and neutrino bremsstrahlung (Dicus *et al.* 1976; Cazzola, De Zotti, and Saggion 1971). The Weinberg-Salam theory with a Weinberg angle of $\sin^2 \theta_W = 0.23$ is applied using Dicus's (1972) formulae and electron, muon, and tau neutrinos are included. For convection, the usual mixing-length theory (cf. Cox and Giuli 1968) with the mixing length put equal to a unit scale height of pressure is employed for the static hydrogen-rich envelope, while a time-dependent mixing-length theory as formulated by Unno (1967) is applied to the core.

III. GRAVITATIONAL CONTRACTION OF NEON STARS AND THE CRITICAL MASS FOR NEON IGNITION

As summarized in § I, whether neon burning is ignited or not is crucial for the evolutionary fate of stars with masses around 10 $M_\odot$. This depends on the mass of O + Ne + Mg core and the degree of electron degeneracy in the central region, since electron degeneracy affects global thermodynamics of the stellar core.

Therefore, it is useful to employ a very simple model of a pure neon star and demonstrate the relation between neon ignition and the mass of neon stars. Such a simple model calculation has been made for stars of hydrogen (Kumar 1963), helium (Cox and Salpeter 1964), and carbon (Murai *et al.* 1968). It has been found that there exists a critical mass below which nuclear fuel is not ignited; the values are 0.08 $M_\odot$, 0.31 $M_\odot$, and 1.06 $M_\odot$ for hydrogen, helium, and carbon burning, respectively.

I computed gravitational contraction of pure neon stars with masses of 1.30 $M_\odot$, 1.35 $M_\odot$, 1.365 $M_\odot$, 1.37 $M_\odot$, and 1.39 $M_\odot$. The initial central density is assumed to be $\rho_c \approx 4 \times 10^4$ g cm^{-3}. Evolutionary tracks in the (ρ_c, T_c) plane are shown in Figure 1 for 1.30 $M_\odot$, 1.365 $M_\odot$, and 1.37 $M_\odot$. The behavior of (ρ_c, T_c) during the contraction can be understood as follows:

During early phase of contraction, electrons are not degenerate and thus the gravothermal specific heat of a star is negative (e.g., Kippenhahn 1970; Sugimoto, Eriguchi, and Hachisu 1981). Therefore, the central temperature increases as heat is removed from the star by radiative transport and neutrino emission; i.e., the gravitational energy release dominates over heat loss.

During later phases, electrons become degenerate and the temperature dependence of the pressure becomes weak. This makes the gravitational energy release inferior to the heat loss and the sign of gravothermal specific heat changes from negative to positive (Kippenhahn 1970; Sugimoto, Eriguchi, and Hachisu 1981); the central temperature of the contracting star begins to decrease.

As seen in Figure 1, T_c attains a peak value which is plotted as a function of the neon star mass, M, in Figure 2; it is shown that the peak value is higher for larger M.

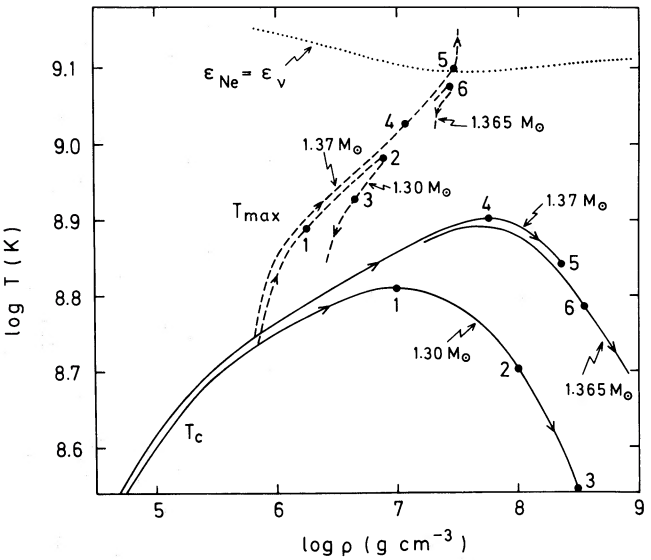

FIG. 1.—Gravitational contraction of pure neon stars with masses $M = 1.30\ M_\odot$, $1.365\ M_\odot$, and $1.37\ M_\odot$. Solid curves show the change in the central temperature, T_c, as a function of the central density; dashed curves show the change in the maximum temperature, T_{max}, throughout the star as a function of the density, ρ, at the shell of T_{max}. Stage numbers (1–6) attached to these curves indicate the same stages. T_c attains its peak value at stages 1 and 4 for $M = 1.30\ M_\odot$ and $1.37\ M_\odot$, respectively; stages 2 and 6 correspond to the peak value of T_{max} for $M = 1.30\ M_\odot$ and $1.365\ M_\odot$, respectively. The dotted line is the ignition line for neon burning. Off-center neon ignition occurs only for neon stars of $M \geq 1.37\ M_\odot$.

When both effects of electron degeneracy and neutrino loss become significant, a temperature inversion appears and a shell of maximum temperature, T_{max}, within the star shifts outward during the contraction. This is due to the density dependence of the plasmon-neutrino emission rate and the weak temperature dependence of the electron-degenerate gas pressure.

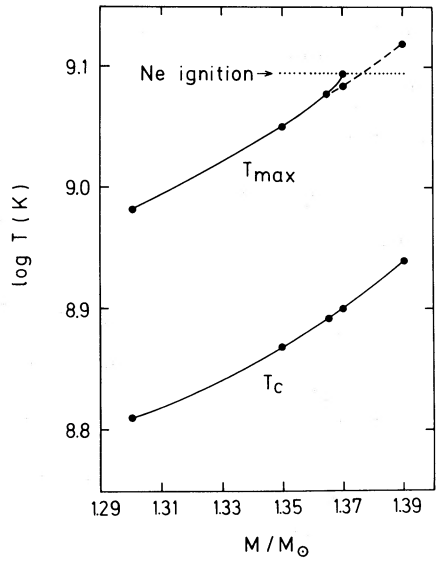

FIG. 2.—The peak values of T_c and T_{max} given in Fig. 1 are shown as a function of neon star mass, M. Dashed curves are obtained by suppressing neon burning. The dotted line indicates the neon ignition line.

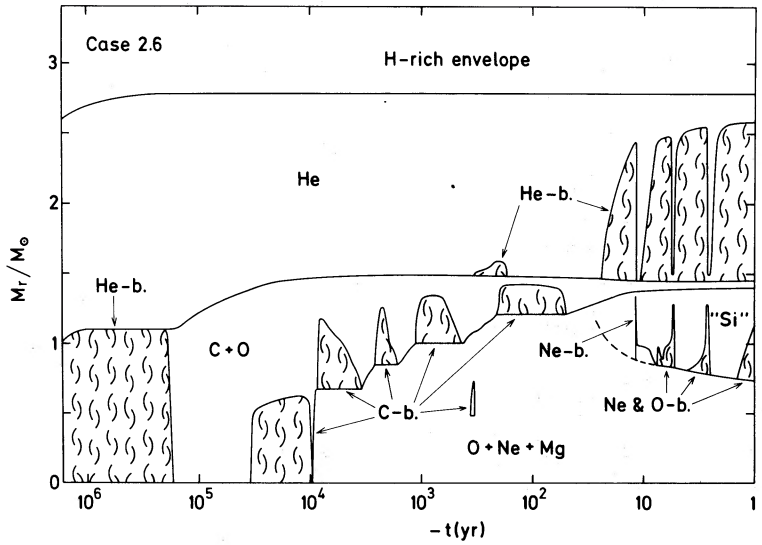

FIG. 3.—Chemical evolution for case 2.6 from helium burning through neon-oxygen shell flashes. The time, t, is measured from the end of the calculation. Curled regions are convective owing to nuclear burning. The upper part of the hydrogen-rich envelope is omitted from the figure.

In Figure 1, the dashed curves show the evolutionary changes in T_{max} against the density of the shell at the location of T_{max} for $M = 1.30\ M_\odot$, $1.365\ M_\odot$, and $1.37\ M_\odot$. For $M \leq 1.365\ M_\odot$, T_{max} rises during the early phase of contraction and then starts to decline before neon ignition. The peak value of T_{max} is plotted against M in Figure 2. The dashed line for T_{max} extending through $M = 1.39\ M_\odot$ is obtained by artificially suppressing neon burning. (The numbers associated with different stages along the curves in Fig. 1 indicate the same stages for T_c and T_{max}).

For $M = 1.37\ M_\odot$, T_{max} reaches the ignition temperature of neon burning at the shell of $M_r = 0.84\ M_\odot$ with $\rho = 3 \times 10^7$ g cm^{-3}. In Figure 2, the neon ignition line is defined by $\epsilon_n = \epsilon_\nu$, where ϵ_n and ϵ_ν denote the nuclear energy generation rate and neutrino emission rate, respectively. As will be discussed in § V, neon shell burning is unstable to a flash and so the temperature rises rapidly.

From Figure 2, we can conclude that the critical mass for neon ignition is $1.37\ M_\odot$ below which neon is not ignited because of electron degeneracy and neutrino cooling. This result is consistent with the conclusion by Boozer, Joss, and Salpeter (1973) who calculated the evolution of C+O stars and estimated the critical mass of C+O stars for neon ignition to be 1.37–1.39 $M_\odot$. This agreement implies that the critical mass does not depend on the details of the core structure.

[It is noteworthy that, in the late stages of evolution of these hypothetical neon stars, the surface layer expands greatly and probably causes mass loss from the star. This is because the luminosity near the surface approaches the local Eddington limit, L_{Ed}, since the Compton scattering opacity increases outward as temperature decreases and, thus, L_{Ed} decreases outward. This mechanism of mass loss due to the temperature dependence of Compton scattering opacity has been found by D. Sugimoto (1970, private communication) in his neon star calculation and applied to a model for mass loss from neutron stars associated with X-ray bursters (Ebisuzaki, Hanawa, and Sugimoto 1983).]

IV. EVOLUTION THROUGH O+Ne+Mg CORE FORMATION

a) General Picture of Evolution

Before discussing the details of the results, I shall describe general features of the evolution of the present models. In Figures 3 and 4, the chemical evolution of the core, i.e., the change in the chemical composition due to nuclear burning, is shown for cases 2.6 and 2.4, respectively. The time, t, is measured from the end of the calculation and $t^* = -t$ is used hereafter. The curled regions are convective owing to nuclear burning.

The cores of the two cases evolve similarly through the phases of helium burning, carbon burning, and the growth of the O+Ne+Mg core with convective carbon shell burning. The characteristic evolutionary stages are summarized in Table 1, where t^* and the masses contained interior to the shell with the maximum energy generation, ϵ_n, for hydrogen

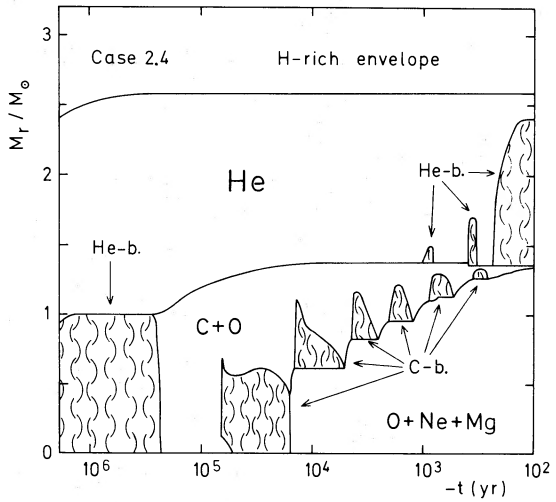

FIG. 4.—Same as Fig. 3 but for case 2.4 from helium burning up to the onset of the dredge-up of the helium layer.

TABLE 1

EVOLUTIONARY STAGES AND CORE MASSES

Stage	Case 2.6 Time[a] t^* (yr)	Case 2.6 Core Mass ($M_\odot$)[b] M_H	M_{He}	M_C	Case 2.4 Time[a] t^* (yr)	Case 2.4 Core Mass ($M_\odot$)[b] M_H	M_{He}	M_C
Beginning of helium burning	1.68 E6	2.60	...	...	1.89 E6	2.40	...	...
Helium exhaustion	1.69 E5	2.79	1.10	...	2.49 E5	2.58	1.02	...
Carbon ignition	3.45 E4	...	1.37	...	6.68 E4	...	1.25	...
Carbon exhaustion	9.73 E3	...	1.44	0.67	1.52 E4	...	1.35	0.61
Carbon shell burning:								
1st peak	8.48 E3	...	1.44	0.67	1.41 E4	...	1.36	0.62
2nd peak	2.52 E3	...	1.48	0.85	4.38 E3	...	1.37	0.84
3rd peak	1.02 E3	...	1.49	0.97	1.91 E3	...	1.38	0.96
4th peak	1.96 E2	...	1.49	1.21	8.51 E2	...	1.38	1.13
5th peak	...	...	...	...	3.47 E2	...	1.35	1.26
Neon ignition	1.19 E1	...	1.45	1.38	...	...	...	...
Onset of dredge-up of He layer	...	...	...	...	5.96 E1	2.581	1.343	1.339
	0.0	2.791	1.449	1.403	...	...	...	...

[a] Time, $t = -t^*$, is measured from the end of the calculation.

[b] Subscripts H, He, and C denote the shell of maximum energy generation of hydrogen, helium, and carbon burning, respectively.

(M_H), helium (M_{He}), and carbon (M_C) burning are given. At later phases, however, the evolution is different for these two cases; i.e., neon is ignited in the outer shell for case 2.6, while the O+Ne+Mg core of case 2.4 cools down without neon ignition. Such a difference is due to the small difference in M_C as seen from Table 1 at $t^* = 0$ yr (case 2.6) and 59.6 yr (case 2.4): For case 2.6, M_C is larger than the critical core mass (1.37 $M_\odot$) for neon burning, while M_C is smaller than 1.37 $M_\odot$ for case 2.4.

In the following sections, the evolution of both cases is discussed phase by phase. Time scales for these phases are obtained from Table 1. Evolutionary changes in the photon luminosity at the outer edge of the core, $L_{ph} \equiv L_{r,1e}$, and the radius of the core edge, r_1, are shown in Figures 5 (case 2.6) and 6 (case 2.4). Changes in the nuclear energy generation rate (without including L_H), L_n, and the neutrino luminosity, L_ν, are shown in Figures 7 (case 2.6) and 8 (case 2.4). Figures 9 (case 2.6) and 10 (case 2.4) show evolutionary changes in the physical quantities in the core, i.e., central density, ρ_c, central temperature, T_c, and central chemical potential of an electron in units of kT, ψ_c (electron degeneracy parameter). When a temperature inversion appears in the core, the maximum temperature within the core, T_{max}, is also plotted in Figures 9 and 10. Finally the evolutionary path of (ρ_c, T_c) is shown in Figures 11 (case 2.6) and 12 (case 2.4).

b) Helium Burning

During the core helium burning phase, the core mass, M_H, increases from 2.60 $M_\odot$ to 2.79 $M_\odot$ for case 2.6 and from 2.40 $M_\odot$ to 2.59 $M_\odot$ for case 2.4 as the envelope material is processed into helium by hydrogen shell burning. (The luminosity, L_H, of hydrogen shell burning during the early

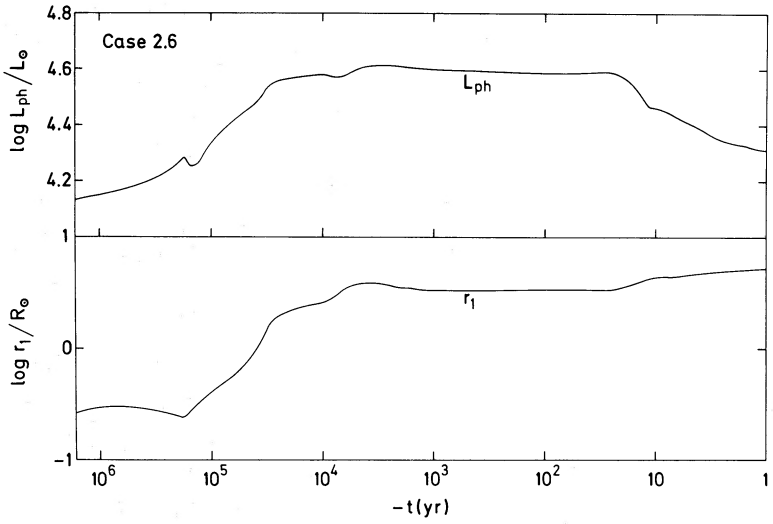

FIG. 5.—Evolutionary changes in the photon luminosity, L_{ph}, and the radial distance from the center, r_1, at the outer edge of the helium layer for case 2.6. Time, t, is the same as in Fig. 1.

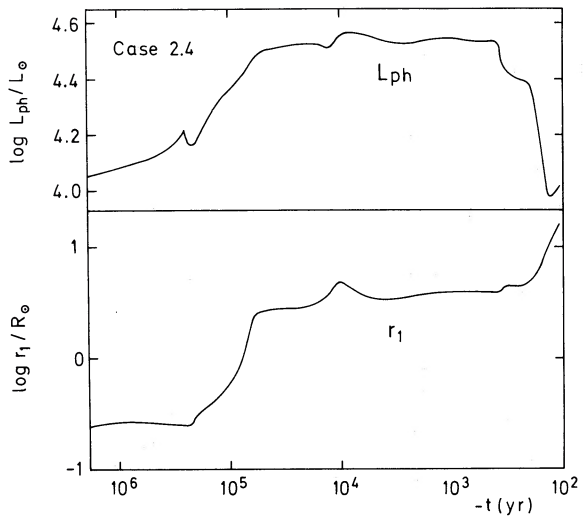

FIG. 6.—Same as Fig. 5 but for case 2.4

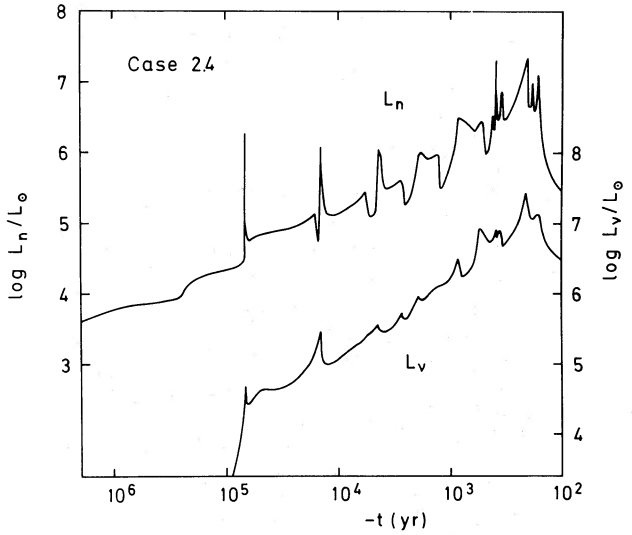

FIG. 8.—Same as Fig. 7 but for case 2.4

stages is obtained from Figs. 5–8 as $L_H = L_{ph} - L_n$). In the later stages of this phase, the outer core edge expands to extinguish hydrogen shell burning and the increase in M_H is stopped.

The quantitative features of this phase agree approximately with previous results (see, e.g., Arnett 1972*a*).

c) Contraction of C+O *Core*

After exhaustion of helium, the star enters the phase of gravitational contraction of the C+O core. A helium-burning shell appears at the outer edge of the former convective core of helium burning (Table 1). The burning shell advances in mass to increase the C+O core mass, M_{He}, up to the value given in Table 1 (see Figs. 3 and 4). The contracting core evolves with increasing T_c and ρ_c (from $\sim 10^4$ to 10^6 g cm^{-3}) as seen in Figures 9–12.

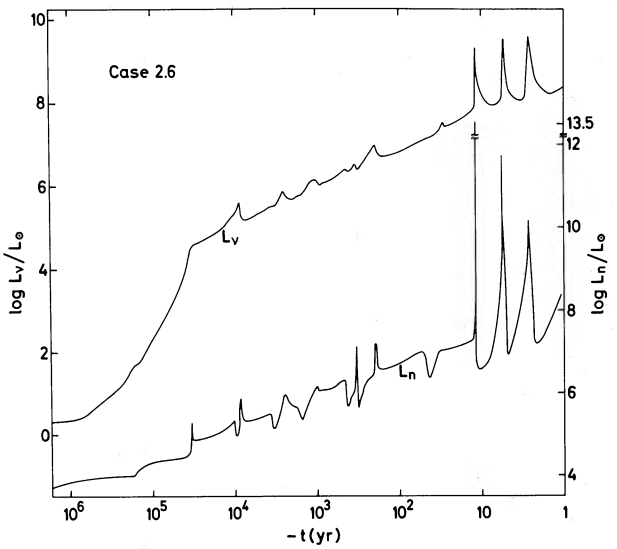

FIG. 7.—Evolutionary changes in the nuclear energy generation rate, L_n, and the neutrino luminosity, L_ν, for case 2.6. Hydrogen shell burning is not included in L_n.

At the same time ($t^* \sim 10^5$ yr), the helium layer expands; r_1 increases by a factor of 6 for case 2.6 (Fig. 5) and of 10 for case 2.4 (Fig. 6). This is essentially the same phenomenon as occurs in a star which evolves from the main sequence to a red giant (Sugimoto and Nomoto 1980, p. 166). During the expansion, entropy in the helium layer increases by absorbing heat from the interior and the photon luminosity, L_{ph}, increases by a factor of 2 (Figs. 5 and 6).

The entropy in the central region decreases mainly by neutrino emission, although the integrated neutrino luminosity, L_ν, is still smaller than L_{ph} (Figs. 7 and 8). Then electrons become degenerate near the center as seen from the increase in ψ_c (Figs. 9 and 10).

Such neutrino cooling in a semidegenerate state yields a slight temperature inversion near the center for case 2.4 when ρ_c is close to 10^6 g cm^{-3} (Fig. 13). This is because the neutrino emissivity is larger for higher density and because the weak temperature dependence of the pressure allows the temperature inversion to exist as mentioned in § III. For case 2.6, such a temperature inversion does not appear during this phase because of the weaker electron degeneracy. The neutrino bremsstrahlung process around $\rho \sim 10^6$ g cm^{-3} is not negligible in determining such a temperature profile.

d) Carbon Burning

During the gravitational contraction, the mass of the C+O core (M_C) exceeds the critical mass for nondegenerate carbon ignition (1.06 $M_\odot$) for both cases. Eventually the contraction results in the ignition of carbon to yield a spike of L_n in Figures 7 and 8.

i) *Case 2.6*

For case 2.6, carbon is ignited at the center when the evolutionary path of (ρ_c, T_c) reaches the ignition line of $\epsilon_n = \epsilon_\nu$ at $\rho_c = 1.0 \times 10^6$ g cm^{-3} in Figure 11.

A convective core develops and the central region expands to reduce ρ_c by a factor of 2 by absorbing heat. Afterwards, the core is almost stationary at $\rho_c \sim 4 \times 10^5$ g cm^{-3} and $T_c \sim 7 \times 10^8$ K until the carbon burning reduces the concentration of carbon in the convective core to $X_C = 0.001$.

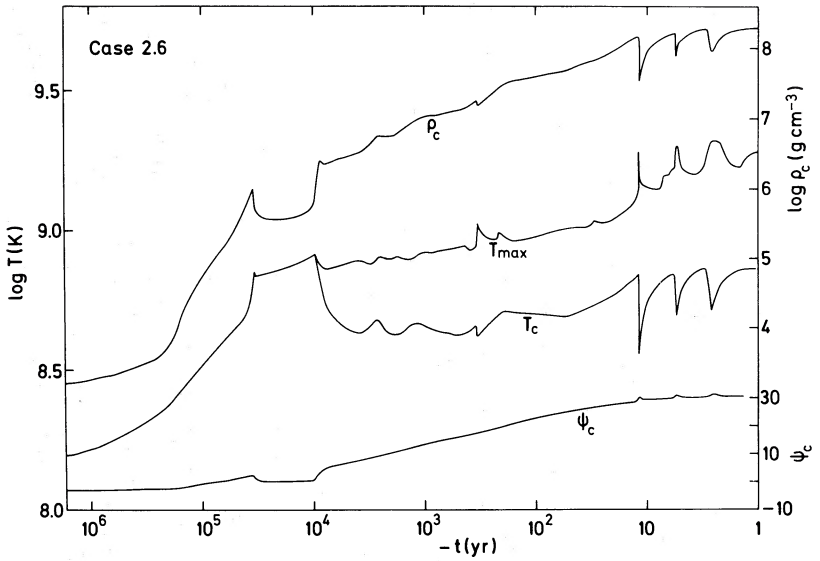

FIG. 9.—Evolutionary changes in the central density, ρ_c, central temperature, T_c, maximum temperature, T_{max}, throughout the core, and chemical potential of an electron at the center, ψ_c, in units of kT for case 2.6.

ii) *Case 2.4*

For case 2.4, carbon ignition occurs at the outer shell of $M_r = 0.045\ M_\odot$ with $T = 5.7 \times 10^8$ K and $\rho = 1.5 \times 10^6$ g cm^{-3} because of the temperature inversion. The temperature profile at this stage is shown against M_r in Figure 13 (*dashed line*) and against ρ by the dashed line near the carbon ignition line in Figure 12.

Such an off-center carbon ignition occurs also for the core of $M_H^{(0)} = 2.2\ M_\odot$ at $M_r = 0.21\ M_\odot$ (Paper II; Nomoto *et al.* 1982). These results are consistent with those found previously (Murai *et al.* 1968; Kutter and Savedoff 1969; Sugimoto 1971; Boozer, Joss, and Salpeter 1973; Ergma and Vilhu 1978; Becker and Iben 1980).

The carbon shell burning is weakly unstable to a flash because of electron degeneracy ($\psi_c \sim 3$), and L_n reaches $2 \times 10^6\ L_\odot$ (Fig. 8). The convective shell extends to $M_r = 0.69\ M_\odot$. The temperature of the flashing shell rises up to 7.2×10^8 K and the density of the overlying layer decreases by a factor of 4. This causes an expansion of the central region and the decrease in ρ_c and T_c in Figures 10 and 12. Afterwards the carbon-burning layer shifts inward as the temperature of the inner layer is raised by heat transport. Then T_c increases and makes a loop around $\rho_c \sim 10^6$ g cm^{-3} in Figure 12. Eventually carbon burning is ignited at the center and proceeds under nondegenerate condition at $\rho_c \sim 4 \times 10^5$ g cm^{-3}. Further evolution is quite similar to case 2.6.

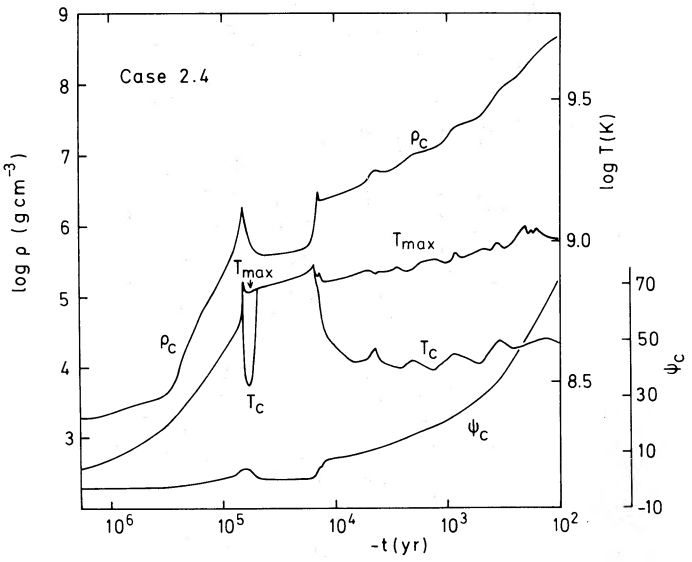

FIG. 10.—Same as Fig. 9 but for case 2.4

e) Growth of O+Ne+Mg *Core*

i) *Temperature Inversion*

When the carbon concentration in the central region is reduced to $X_C = 0.001$, the core starts to contract as seen from the increase in ρ_c around $t^* \approx 10^4$ yr (Figs. 9 and 10). After exhaustion of carbon, a core of O+Ne+Mg is left which enters a phase of gravitational contraction.

The entropy in the central region is reduced by the neutrino emission and the electron degeneracy increases. Such cooling in the electron degenerate state causes a substantial decrease in T_c at $t^* \approx 10^4$ yr (Figs. 9 and 10).

At the formation of O+Ne+Mg core, a carbon-burning shell appears at $M_r = M_C$ as given in Table 1. The shell of maximum temperature, T_{max}, within the core moves from the center to the carbon-burning shell because of cooling of the central core; in other words, a large temperature inversion appears as seen from T_{max} and T_c in Figures 9 and 10.

ii) *Convective Carbon Shell Burning*

During the carbon shell burning phase, $L_n \approx L_\nu$ holds (Figs. 7 and 8). Because of the stronger temperature dependence of ϵ_n than that of ϵ_ν, however, ϵ_n exceeds ϵ_ν at the bottom of the carbon-burning shell. Accordingly, a convective shell develops to carry the excess energy outward.

As carbon is depleted, the convective shell shrinks and disappears. A radiative phase then follows and the shell of

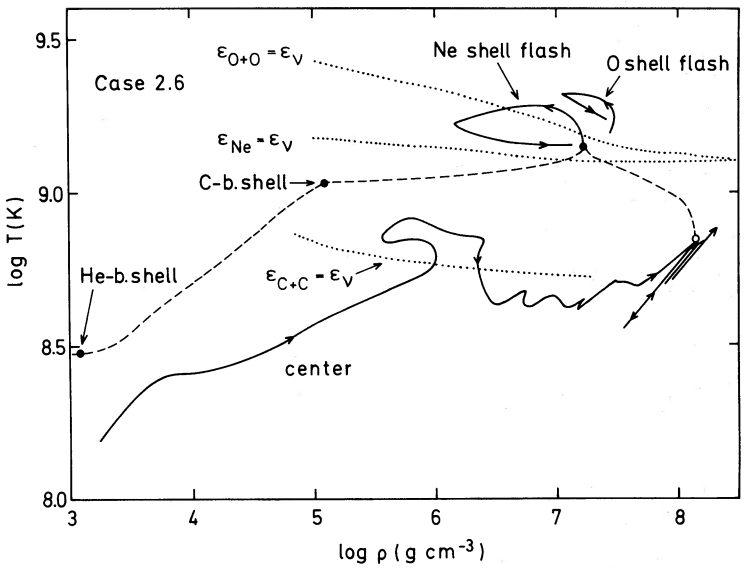

FIG. 11.—Evolutionary tracks of the central density and temperature for case 2.6 are shown by the solid line. At neon ignition, the temperature profile against log ρ is shown by the dashed curve, where the open and filled circles indicate the center and the burning shells of neon, carbon, and helium, respectively. Evolutionary paths of (ρ, T) at the neon flashing shell and the oxygen flashing shell are shown by the solid curve. Dotted lines indicate the ignition lines of carbon, neon, and oxygen.

maximum ϵ_n advances in Lagrangian coordinate, M_r, in the region of small X_C where $\epsilon_n < \epsilon_\nu$. Eventually the carbon-burning shell reaches a shell with relatively large X_C; then ϵ_n exceeds ϵ_ν and a convective shell appears. Such a convective carbon-burning shell appears repeatedly as seen from Figures 3 and 4. In Table 1, epochs at the peak L_n for each convective phase are given.

In the Eulerian coordinate, r, the carbon-burning shell stays around $r \approx 10^{-2} R_\odot$ throughout the shell-burning phase; during the radiative phase, a layer with large X_C contracts until the density and temperature there become high enough to ignite carbon.

The convective shell never touches the tail of helium layer. The entropy difference between the helium layer and the convective layer would require additional energy release of as much as 2×10^{17} ergs g^{-1} for the mixing of helium to occur.

The energy generation rate of carbon shell burning does not exceed $2 \times 10^7 L_\odot$ (Figs. 7 and 8) which is too weak to induce any dynamical effects.

For case 2.6, some carbon, which remains unburned in the O+Ne+Mg core, is ignited (i.e., $\epsilon_n > \epsilon_\nu$) at $t^* \approx 300$ yr as the temperature rises during the contraction. This gives rise to an irregular behavior of L_n, ρ_c, T_c, T_{max}, etc. but does not cause a major effect on the evolution. For case 2.4, the

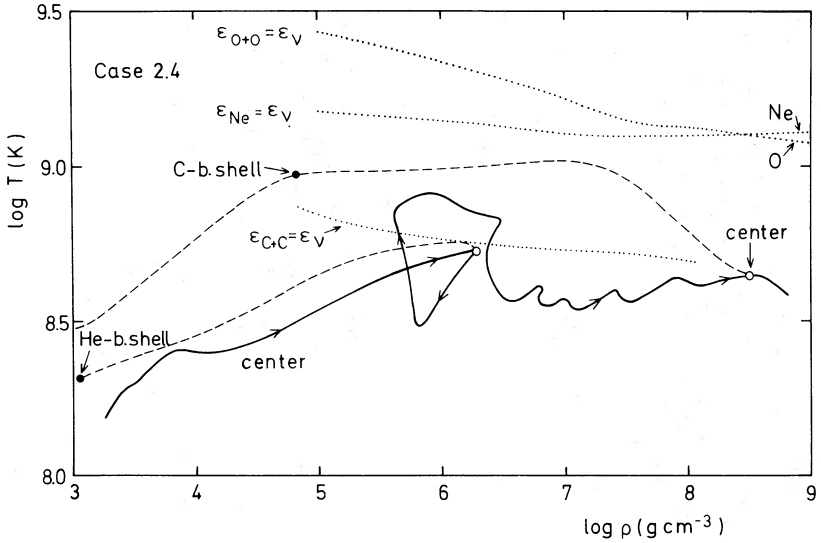

FIG. 12.—Same as Fig. 11 but for case 2.4. Dashed lines show the temperature profiles at carbon ignition and at $t^* = 140$ yr when T_{max} attains its peak value.

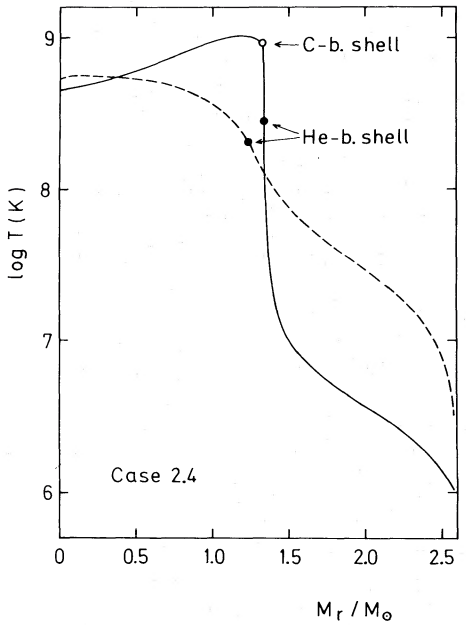

FIG. 13.—Temperature profiles against M_r for case 2.4 at off-center carbon ignition (dashed curve; $t^* = 6.68 \times 10^4$ yr) and at the stage when T_{max} attains the peak value (solid curve; $t^* = 140$ yr). Filled and open circles indicate the burning shells of helium and carbon, respectively.

carbon in the O+Ne+Mg core burns relatively peacefully without developing a convective shell, and small amount of carbon remains unburned.

iii) *Temperature Change during the Core Growth*

Through the phase of carbon shell burning, the mass of the O+Ne+Mg core grows gradually (Table 1), and ρ_c and ψ_c increase. On the other hand, the maximum temperature, T_{max}, in the outer shell increases only slightly (Figs. 9 and 10), since T_{max} is determined by the balance of $L_n \approx L_\nu$ at the carbon-burning shell. Also T_c stays around 4×10^8 K which is determined by the balance between compression of the central region and the neutrino energy loss.

Small irregularities in these quantities as seen in Figures 9 and 10 are due to the onset of convective carbon shell burning: the expansion of the carbon burning shell makes the core contraction slower and compressional heating smaller. As a result, T_c decreases because of the neutrino emission.

V. OFF-CENTER NEON FLASH FOR CASE 2.6

a) *Temperature Profile*

After the fourth convective carbon shell burning for case 2.6, the mass of the O+Ne+Mg core, M_C, grows to approach $M_{He} = 1.45\ M_\odot$ ($t^* \approx$ 50–10 yr). This implies M_C can exceed the critical mass of 1.37 $M_\odot$ for neon ignition. The core is relativistically degenerate so that ρ_c increases rather rapidly as M_C increases.

When M_C becomes 1.30 $M_\odot$, the shell of T_{max} shifts inward from the carbon burning shell ($M_r = M_C$) to $M_r = 1.0\ M_\odot$. Such a change in the temperature profile is caused by the density dependence of the neutrino loss rate (mainly pair and photo neutrino processes) which is larger near the outer edge of the O+Ne+Mg core ($\rho \sim 10^5$ g cm^{-3}) than in the layer of $M_r \sim 1.0\ M_\odot$. In still deeper layers of the core, the compressional heating due to contraction is less effective.

The temperature profile at neon ignition (see § IV*b*) is shown against ρ in Figure 11 (*dashed line*) and against M_r in Figure 14.

b) *Neon Shell Flash*

When M_C reaches 1.38 $M_\odot$ ($t^* = 12$ yr), neon is ignited at the shell with $M_r = 0.88\ M_\odot$ ($\rho = 1.8 \times 10^7$ g cm^{-3}). Since electrons at the ignited shell are somewhat degenerate, i.e., $\psi \approx 5$, neon shell burning is unstable to a flash. The temperature rises up to 2×10^9 K and then declines because of the expansion of the flashing shell. When the burning shell expands to $\rho = 1.4 \times 10^6$ g cm^{-3}, the neutrino energy loss rate (L_ν) exceeds the energy generation rate of neon burning (L_n). Then the shell starts to lose entropy and contract. Accordingly, the evolutionary path of the density and temperature of the neon burning shell makes a loop in (ρ, T) plane as seen in Figure 11.

Although the increase in temperature is only a factor of 1.5, L_n increases by a factor of 10^6 and reaches $3.5 \times 10^{13}\ L_\odot$ because of the strong temperature dependence of the neon burning rate. The peak value of L_n for this neon flash is much higher than for helium shell flashes (e.g., $L_{He} \sim 10^7\ L_\odot$ for a 1.39 $M_\odot$ C+O core; Sugimoto and Nomoto 1975) and carbon shell flashes (e.g., $L_{C+C} \sim 6 \times 10^8\ L_\odot$ for 1.1 $M_\odot$ C+O core; Sugimoto 1971), but it is too weak to induce dynamical effects. In fact, the time scale of expansion at the flashing shell is $-dt/d \ln \rho \sim 400$ s which is 10^3 times longer than the dynamical time scale.

A convective shell of neon burning develops extending from $M_r = 0.88\ M_\odot$ to 1.34 $M_\odot$. At the stage of its maximum extent when neon has been almost depleted ($X_{Ne} = 0.03$), the outer edge of the convective shell touches the tail of the carbon layer with $X_C \lesssim 5 \times 10^{-4}$. However, the amount of carbon mixed into the convective layer is too small to give rise to appreciable effect. In order for the convective shell to reach

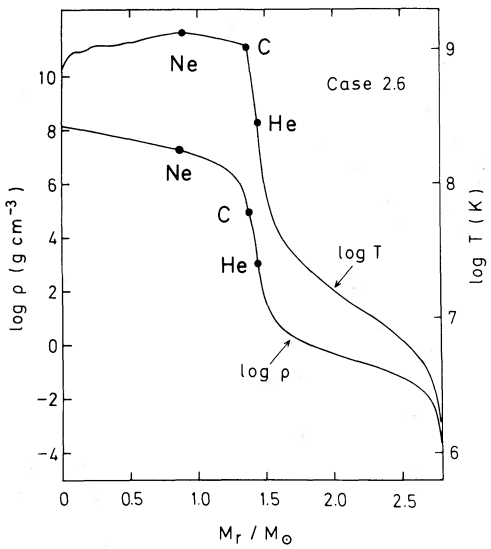

FIG. 14.—Density and temperature profiles against M_r for case 2.6 at neon ignition ($t^* = 11.9$ yr). Filled circles indicate the nuclear burning shells.

the carbon layer with $X_C \gtrsim 0.1$, an additional nuclear energy release of more than 10^{17} ergs g^{-1} would be required, i.e., more neon with $X_{Ne} \sim 0.2$ in the shell should have burned. Thus it is unlikely that the carbon and neon layers are mixed enough to affect further evolution.

c) *Oxygen Shell Flash*

After the first neon flash ceases, heat is transported inward to ignite the next neon flash at the shell with $M_r = 0.87\ M_\odot$. Because of its small concentration, neon is quickly exhausted and an oxygen flash follows. This flash develops a convective layer extending to $M_r = 1.28\ M_\odot$. The change in (ρ, T) at the oxygen-flashing shell is shown in Figure 11. The temperature peak is only slightly higher than for the previous neon flash and thus L_{O+O} is smaller than L_{Ne} (Fig. 11). Therefore L_ν exceeds L_{O+O} (i.e., the entropy starts to decrease) shortly after the peak temperature is attained and the flash makes a smaller loop in the (ρ, T) plane than does the neon flash. These neon-oxygen shell flashes occur successively in the inner shell as seen from Figures 3 and 7.

However, the behavior of these flashes may depend sensitively on zoning. Since a more careful treatment seems to be needed, the calculation was stopped when the neon-flashing shell reached the shell with $M_r = 0.7\ M_\odot$.

During the developing phase of these shell flashes (i.e., the phase with $L_n > L_\nu$), the shell-burning layer expands and the pressure there decreases by a factor of 17 during the neon flash. Such a pressure decrease in the shell causes an almost adiabatic expansion of the central core and the decrease in both ρ_c and T_c as shown in Figures 9 and 14. When the burning shell contracts (i.e., $L_n < L_\nu$), the central core also contracts.

The above features of neon-oxygen shell flashes are similar to those that occur in a 15 $M_\odot$ star with $M_{He} = 1.7\ M_\odot$ (Sparks and Endal 1980) and in a 10 $M_\odot$ star with $M_{He} = 1.5\ M_\odot$ (Woosley, Weaver, and Taam 1980).

It is noteworthy that the behavior of the shell flashes described above is now well understood in a generalized fashion (Sugimoto and Miyaji 1981): the rise and decline of temperature at the flashing shell are described in terms of the gravothermal specific heat, c_g, which is a combination of the usual thermodynamic specific heat and a term due to hydrostatic readjustment upon a change of entropy. At the temperature peak of the present flashes, c_g changes from positive to negative because electron degeneracy becomes as weak as $\psi = 1.7$ and the geometry at the burning shell gets closer to spherical; these two effects make expansion easier. This implies that the peak value of the temperature does not depend on the nuclear fuel (neon or oxygen) but depends only on ψ and the geometry at the burning shell. (See Sugimoto and Miyaji 1981 for more detail.)

VI. FORMATION OF A STRONGLY DEGENERATE O + Ne + Mg CORE FOR CASE 2.4

a) *Cooling of the* O + Ne + Mg *Core*

For case 2.4, a convective shell of carbon burning appears repeatedly five times (Fig. 4 and Table 1). After the fifth convective shell, a radiative carbon-burning shell advances from $M_r = 1.26\ M_\odot$ to $1.339\ M_\odot$ (Table 1).

The shell at T_{max} lies at the carbon burning shell until T_{max} attains a peak value of 1.11×10^9 K at $t^* = 160$ yr. The location of T_{max} then shifts to the O + Ne + Mg layer. Subsequent contraction of the core raises T_{max} up to 1.04×10^9 K at the shell with $M_r = 1.18\ M_\odot$ ($t^* = 140$ yr). Afterward, both T_c and T_{max} decrease as ρ_c increases (Fig. 10); electron degeneracy gets stronger and stronger as the core contracts further. At $t^* = 0$, a strongly degenerate O + Ne + Mg core is formed, i.e., $\log \rho_c = 8.82$, $\log T_c = 8.59$, $\psi_c = 92$, and $\log T_{max} = 8.95$ at $M_r = 1.29\ M_\odot$ ($\log \rho = 6.76$).

In Figure 12 (*dashed curve*) and 13 (*solid curve*) are shown the temperature distributions against ρ and M_r at $t^* = 140$ yr. The peak value of T_{max} attained at this stage is smaller than the ignition temperature of neon burning (defined by $\epsilon_n = \epsilon_\nu$) by a factor of 1.2. Thus neon ignition never does occur for case 2.4, which is distinct from case 2.6.

b) *Critical Mass of Helium Core for Neon Ignition*

As discussed in § III, there exists a critical neon star mass of 1.37 $M_\odot$ for neon ignition. We can make the difference between cases 2.6 and 2.4 clear in terms of neon star mass. In Figure 15, the density distribution of case 2.4 at $t^* = 0$ yr is shown by the solid line. A very steep density gradient at the helium burning shell with $M_{He} = 1.34\ M_\odot$ clearly separates the star into a core and an extended helium envelope. Thus the core mass of 1.34 $M_\odot$ can be regarded as a neon star mass for case 2.4. Similarly the density distribution for case 2.6 in Figure 14 indicates that $M_{He} = 1.45\ M_\odot$ is equivalent to a neon star mass.

It should be noted that the increase in M_{He} is negligible during the phase of increasing M_C (i.e., $L_{He} \ll L_{C+C}$); this is because the carbon-burning shell advances rather rapidly in mass at a rate determined by a balance of $L_{C+C} \approx L_\nu$ while L_ν is much smaller in the helium-burning shell because of the

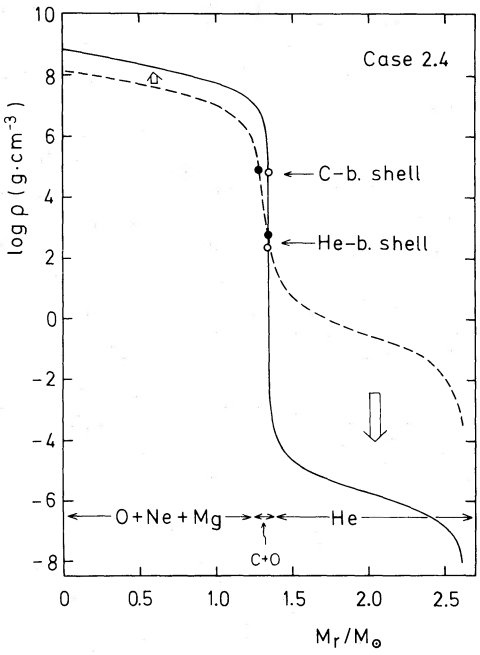

FIG. 15.—Changes in the density distribution from $t^* = 256$ yr (*dashed curve*) to $t^* = 0$ yr (*solid curve*) for case 2.4. Expansion of the helium layer to a red giant size is seen.

lower temperature. Therefore M_{He} remains practically constant.

Whether M_{He} is larger than 1.37 $M_\odot$ or not is crucial for neon ignition, and this is why neon is ignited for case 2.6 but not for case 2.4. The core mass of $M_H^{(0)} = 2.5\ M_\odot$, which corresponds approximately to the stellar mass of 10 $M_\odot$, is about the critical mass for neon ignition.

c) *Expansion of the Helium Layer*

At $t^* = 256$ yr when M_C reaches 1.27 $M_\odot$, the helium layer starts to expand greatly. As seen from Figure 6, the radius at the outer edge of the helium layer, r_1, increases from 4.4 $R_\odot$ ($t^* = 256$ yr) to 38 $R_\odot$ ($t^* = 59.6$ yr). Since the hydrogen-rich envelope has a deep surface convection zone, such an expansion of the helium layer leads to the penetration of the convection zone into the helium layer at $t^* = 59.6$ yr.

By suppressing the penetration of the surface convection zone into the helium layer, the expansion was calculated up to $t^* = 0$ yr when r_1 reaches 190 $R_\odot$, almost red-giant size. The change in the density distribution from $t^* = 256$ yr (*dashed line*) to 0 yr (*solid line*) is shown in Figure 15, which clearly shows a transition of the helium layer to the red-giant–like envelope with an average density of as low as $\sim 10^{-6}$ g cm^{-3}. This expansion is driven by the core contraction with the increase in ρ_c by a factor of 5.5. During the expansion, L_{ph} decreases by a factor of 3 (Fig. 6) since energy is used for the expansion.

The mechanism of such an envelope expansion associated with the core contraction is essentially the same as of the evolution from a main-sequence star to a red-giant (Sugimoto and Nomoto 1980, p. 166). The extent of the helium envelope expansion depends on the mass of the helium layer as investigated by Joss *et al.* (1973).

Subsequent dredge-up of a helium layer has not been calculated yet for case 2.4 but should be similar to the case of $M_H^{(0)} = 2.2\ M_\odot$ (Nomoto *et al.* 1982; Nomoto 1983). It has been found that the penetration of the surface convection zone continues until almost all the helium layer is dredged up and the hydrogen shell burning becomes active; afterward, the star enters the phase of hydrogen-helium double shell burning. The early phase of dredge-up during the growth of the O+Ne+Mg core was calculated for a 9 $M_\odot$ star by Weaver, Axelrod, and Woosley (1980), which is consistent with the case of $M_H^{(0)} = 2.2\ M_\odot$. The dredge-up in these cases is similar to that which occurs for C+O cores in 6–8 $M_\odot$ stars (e.g., Paczyński 1970; Sugimoto 1971; Becker and Iben 1979).

VII. COMPOSITION STRUCTURE

The composition structure at $t^* = 0$ yr for case 2.6 and $t^* = 59.6$ yr for case 2.4 are shown in Figures 16 and 17, respectively. The mass coordinate in these figures is scaled up by a factor of 10 for 1.40 $M_\odot \le M_r \le 1.45\ M_\odot$ (case 2.6) and a factor of 80 for 1.335 $M_\odot \le M_r \le 1.345\ M_\odot$ (case 2.4) because the carbon- and helium-burning layers are very thin in mass.

a) *Core of Heavy Elements*

Interior to the carbon burning shell at $M_r = 1.403\ M_\odot$ (case 2.6) and 1.339 $M_\odot$ (case 2.4), a core of O+Ne+Mg is formed. Neon is the most abundant species and X_{Ne}, X_{Mg}, and X_{Ne}/X_O in the central region are larger for smaller core mass. This tendency is due to the smaller T_c for smaller mass cores during carbon burning and is consistent with the results for 15–25 $M_\odot$ stars by Arnett (1972*b*), Endal (1975*a*, *b*), Lamb, Iben, and Howard (1976), and Weaver, Zimmermann, and Woosley (1978). The difference between off-center ignition and central ignition might also affect the composition. In the present models, stellar masses are smaller than the previous massive star models, so that there would be some ^{23}Na (Arnett 1973; Endal 1975*a*; Lamb, Iben, and Howard 1976). Thus the composition in Figures 16 and 17 assuming the steady abundance of ^{23}Na must be considered approximate.

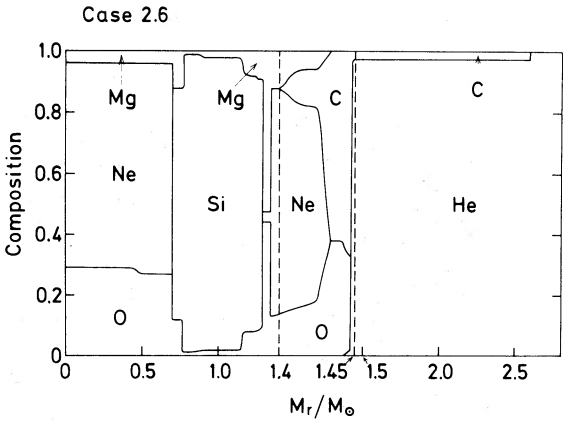

FIG. 16.—Composition structure at $t^* = 0$ yr for case 2.6. Concentration by weight is shown. The abscissa is scaled up by a factor of 10 for 1.40 $M_\odot \le M_r \le 1.45\ M_\odot$.

For case 2.6, there exists a layer of neon-oxygen burning products, mainly Si-rich elements, above the O+Ne+Mg core. As mentioned in § V, the calculation of neon-oxygen shell flashes and the nuclear products are preliminary.

Above the carbon-burning shell, there is a very thin C+O layer. The layer is thinner for the smaller mass star, i.e., 0.046 $M_\odot$ for case 2.6 and 0.004 $M_\odot$ for case 2.4. The C+O layer in case 2.4 will grow during the subsequent hydrogen-helium double shell burning as found for the core of $M_H^{(0)} = 2.2\ M_\odot$ (Nomoto 1983). On the other hand, further evolution

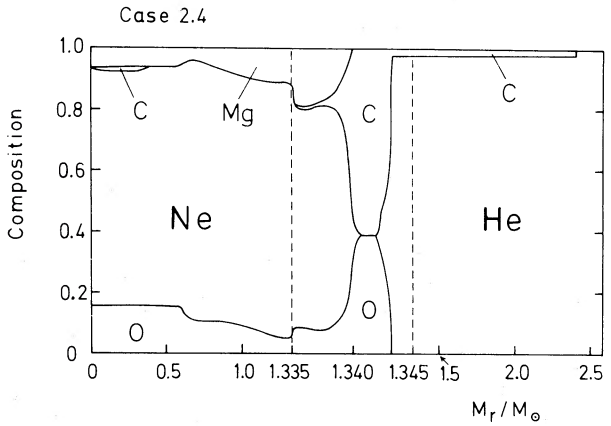

FIG. 17.—Same as Fig. 15 but for case 2.4 at $t^* = 59.6$ yr. The abscissa is scaled up by a factor of 80 for 1.335 $M_\odot \le M_r \le 1.345\ M_\odot$.

of case 2.6 may be too rapid for the carbon-burning shell to advance appreciably.

b) Helium Layer

The composition of the helium layer changes at a late phase of evolution for both cases. As seen in Figures 3 and 4, helium shell burning becomes active and develops a convective zone which extends through most of the helium layer, i.e., from $M_r = 1.449\ M_\odot$ to $2.60\ M_\odot$ (case 2.6) and from $M_r = 1.343\ M_\odot$ to $2.40\ M_\odot$ (case 2.4). During the active phase of convective helium burning, the shell of maximum energy generation, which is indicated by the solid line separating the C+O and He layers in Figures 3 and 4, moves inward by $\Delta M_r \sim 0.04\ M_\odot$ (Table 1) following the core contraction.

As a result, some amount of carbon (and a small amount of oxygen also) in the helium-burning region are dredged up into the convective zone, and moreover, helium burning under these conditions processes helium mainly into carbon. At the end of the calculation, the concentration of carbon in the convective zone is $X_C = 0.027$ (case 2.6) and 0.022 (case 2.4), and the oxygen concentration is $X_O = 0.0036$ (case 2.6) and 0.0033 (case 2.4).

Such carbon production in the convective helium burning shell occurs commonly for the late stage of evolution of massive stars (Arnett 1974*b*; Weaver, Zimmermann, and Woosley 1978; Sparks and Endal 1980; Nomoto 1982*c*), and X_C is larger for more massive stars as summarized by Nomoto (1982*c*), which is consistent with the present tendency.

Whether any such carbon enrichment can be observed at the stellar surface depends on the stellar mass. For case 2.4, the penetrating surface convection zone dredges up carbon as well as helium toward the surface as discussed in § VI. Therefore, if the hydrogen-rich envelope had lost a sufficiently large amount of mass by a stellar wind before the dredge-up, the carbon-to-oxygen ratio would exceed unity in the surface convection zone; then the star would be observed as a carbon star. Such a mechanism to yield carbon stars does not work for stars more massive than case 2.6 because the dredge-up does not take place.

The amount of carbon produced in the helium layer may be too much to be compatible with the relatively small carbon abundance and large helium abundance of the Crab nebula; this is the reason why smaller mass stars are preferable for the Crab nebula's progenitor (Davidson *et al.* 1982; Nomoto 1982*c*; Nomoto *et al.* 1982).

VIII. DISCUSSION

a) Further Evolution for Case 2.6

Previous studies have suggested the following three possibilities for evolutionary paths for case 2.6 after the off-center neon-oxygen burning:

1. The neon-oxygen–burning shell reaches the center peacefully and the resultant Si-rich core may become somewhat degenerate. Such an evolution was found to occur for a $1.5\ M_\odot$ C+O star (Ikeuchi *et al.* 1972) and for a $15\ M_\odot$ star with $M_{He} = 1.7\ M_\odot$ (Sparks and Endal 1980).

2. The neon-oxygen–burning shell does not reach the center and an unburned O+Ne+Mg core may become strongly degenerate as shown by Barkat, Reiss, and Rakavy (1974) for their $8\ M_\odot$ star having a core of $M_{He} \approx 1.4\ M_\odot$.

3. The neon-oxygen–burning shell reaches the center but not peacefully. After the formation of a Si-rich intermediate shell, the core contracts to ignite a violent neon flash in the remaining neon-rich core. Such a complicated evolution was reported by Woosley, Weaver, and Taam (1980) for their $10\ M_\odot$ star with $M_{He} \sim 1.5\ M_\odot$.

The outcome of the neon-oxygen shell burning strongly depends on M_{He} and thus on stellar mass M, since M_{He} varies, crossing the Chandrasekhar limit, as M varies around $10\ M_\odot$. Also, the results may depend on the physical input and zoning in the calculation; thus a systematic study of stars of $M \sim 10\ M_\odot$ is required.

b) Further Evolution for Case 2.4 toward Electron Capture Supernovae

As discussed in § VI, dredge-up of a helium layer by the surface convection zone will occur after $t^* = 59.6$ yr for case 2.4. The evolution from dredge-up phase through the electron capture core collapse has been calculated for a core of $M_H^{(0)} = 2.2\ M_\odot$, which was briefly reported in Nomoto *et al.* (1982) and Nomoto (1983). The evolution of the core of case 2.4 should be similar to this case and thus will be the following.

1. When most of the helium layer is dredged up, the surface convection zone retreats, and the hydrogen shell burning is ignited. The helium layer then grows until an unstable helium shell burning is ignited to make a thermal pulse.

2. Subsequent hydrogen-helium double shell burning with many cycles of helium shell flashes increases the mass of the C+O layer, which leads to the contraction of the O+Ne+Mg core. The growth rate of the C+O layer is too slow to raise the temperature there, so that the carbon shell burning is quenched by the neutrino cooling.

3. During the helium shell flashes, the temperature of the flashing shell gets higher than for 4–8 $M_\odot$ stars with C+O cores since M_{He} is as high as 1.3–1.37 $M_\odot$ for 8–10 $M_\odot$ stars. Thus *s*-process nucleosynthesis based on the $^{22}Ne(\alpha,n)^{25}Mg$ reaction may take place more efficiently than for 4–8 $M_\odot$ stars (Iben 1975; Sugimoto and Nomoto 1975; Iben and Truran 1978).

4. The evolutionary track in the (ρ_c, T_c) plane almost merges into the common track for the degenerate C+O cores of 4–8 $M_\odot$ stars since the growth rate for the core mass (O+Ne+Mg plus C+O) is the same as for a C+O core.

5. When M_{He} exceeds $1.375\ M_\odot$, electron captures on ^{24}Mg and ^{20}Ne trigger the collapse of the core.

Hydrodynamical stages after the onset of electron captures should be the same as reported in detail by Miyaji *et al.* (1980) and Nomoto (1983); the core continues to collapse despite oxygen combustion; i.e., the star evolves into an electron capture supernova.

It must be emphasized that the above evolutionary scenario should be common for stars with cores of $M_H^{(0)} \approx 2.0$–$2.5\ M_\odot$, i.e., for 8–10 $M_\odot$ stars. The basis for this argument is the following: For the 8–10 $M_\odot$ star, a degenerate O+Ne+Mg core is formed after carbon burning. Its later phase of evolution is determined only by the growth rate of the core mass due to hydrogen-helium double shell burning, which is independent of the early evolution and the envelope mass as

has been discussed for the degenerate C+O cores in 4–8 $M_\odot$ stars (Paczyński 1970, 1971; Barkat 1971; see Sugimoto and Nomoto 1980, p. 177, for a review).

c) *Formation of* O+Ne+Mg *White Dwarfs*

i) *Case of Single Stars*

Formation of O+Ne+Mg white dwarfs could be a possible alternative to the electron capture supernovae as a final fate of 8–10 $M_\odot$ stars.

Recently many people have suggested that 4–8 $M_\odot$ stars which develop degenerate C+O cores may lose their entire hydrogen-rich envelope before carbon ignition and leave C+O white dwarfs (see Weidemann 1979 for a review). The upper mass limit of the white dwarf progenitor, $M_{\rm WD}$*, is still uncertain but could be around 8 $M_\odot$.

In this respect, it must be noted that the stellar structure at the double shell burning phase of 8–10 $M_\odot$ stars is essentially the same as for 4–8 $M_\odot$ stars; i.e., the star consists of a red-giant–size hydrogen-rich envelope, a thin helium layer, and a degenerate core. Except for the composition of the degenerate core, the only difference between 4–8 $M_\odot$ stars and 8–10 $M_\odot$ stars is the mass of the hydrogen-rich envelope. Since the luminosity is given by Paczyński's (1970) core mass to luminosity relation, the location of 8–10 $M_\odot$ stars in the H-R diagram (near the Hayashi line) is close to that of 4–8 $M_\odot$ stars during their double shell burning phase.

Accordingly, mass loss from 8–10 $M_\odot$ stars at the pre-collapse phase could be as efficient as that from 4–8 $M_\odot$ stars, and $M_{\rm WD}$* could possibly be as high as 8–10 $M_\odot$. If so, the mass range of 8–10 $M_\odot$ would be divided as follows: Stars of mass 8 $M_\odot$–$M_{\rm WD}$* leave O+Ne+Mg white dwarfs while stars in the mass range $M_{\rm WD}$*–10 $M_\odot$ evolve into electron capture supernovae.

To determine $M_{\rm WD}$* from the theoretical side, it must be taken into consideration that the lifetime of the high-luminosity double shell burning phase (asymptotic giant branch phase) is as short as 4×10^4 yr for case 2.4 which is shorter than for 4–8 $M_\odot$ stars by a factor of at least 15 because the mass of the degenerate O+Ne+Mg core is already as large as 1.34 $M_\odot$ at its formation for case 2.4 [and 1.28 $M_\odot$ for a case of $M_{\rm H}^{(0)} = 2.2\ M_\odot$; Nomoto *et al.* 1982]. Such a lifetime is longer for smaller mass stars, which favors smaller $M_{\rm WD}$*.

It is interesting to note that the mass of an O+Ne+Mg white dwarf must be in the range 1.2–1.37 $M_\odot$, which is much higher than the average mass of 0.6 $M_\odot$ for the field white dwarfs (e.g., Weidemann 1979).

ii) *Case of Close Binaries*

In some close binary systems, the primary star is a 8–10 $M_\odot$ star which could evolve into an O+Ne+Mg white dwarf in the following way (Nomoto *et al.* 1979; Nomoto 1980*a*, 1981).

When the primary star evolves off the main-sequence, its hydrogen-rich envelope is lost by Roche lobe overflow and a helium star of 2–2.5 $M_\odot$ is left. The helium star evolves further to develop a degenerate O+Ne+Mg core as investigated in the present paper. (The difference between the helium star and the helium core is negligible except for the surface layer.) Eventually, the helium envelope expands to a red giant size and is lost by Roche lobe overflow. Then the O+Ne+Mg core with thin C+O and helium layers is left and cools down to a white dwarf.

The above evolutionary scenario involving two-step mass transfer (case BB) is similar to the formation of C+O white dwarfs in close binaries (see Webbink 1979 for a review). The mass range for O+Ne+Mg white dwarfs is 1.2–1.37 $M_\odot$, which is also larger than the average white dwarf mass of $\sim 1\ M_\odot$ in the cataclysmic binaries.

An O+Ne+Mg white dwarf in a close binary system is a potentially important object as a precursor for cataclysmic variables and low-mass X-ray binaries containing accreting neutron stars (e.g., van den Heuvel 1981). When the companion star starts to transfer mass onto the white dwarf, accumulation of the matter would lead to rejuvenation of the cold white dwarf, i.e., ignition of hydrogen shell flashes and a possible increase in the white dwarf mass up to the Chandrasekhar limit.

The differences in the behavior between the O+Ne+Mg white dwarfs and the C+O white dwarfs are summarized as follows (Nomoto 1980*a*, *b*): The hydrogen shell flashes in the O+Ne+Mg white dwarfs should be in general stronger than in C+O white dwarfs because of the larger white dwarf mass. The ultimate result of mass increase is a collapse into a neutron star for O+Ne+Mg white dwarfs, while complete disruption results from C+O white dwarfs, perhaps making a Type I supernova.

d) *Hydrogen-deficient Carbon Stars*

For case 2.4, carbon is produced in the convective shell of helium burning and can be brought to the stellar surface by the dredge-up of the helium layer. As mentioned in § VI, if the mass of the hydrogen-rich envelope is small enough, the star could become a carbon star.

In the extreme case of mass loss, most of the hydrogen-rich envelope could be lost before the onset of dredge-up. Then the helium envelope would expand to a red giant size as seen from Figure 15 and the surface convection zone would become deep enough to mix carbon up to the surface. In such a helium star, $X_{\rm C}$ is apparently larger than $X_{\rm O}$ so that the star would be observed as a hydrogen-deficient carbon star. The relation of such models to R CrB stars (e.g., Cottrell and Lambert 1982) might be worth investigating.

e) *Type II Supernovae or Type I Supernovae?*

Recently, Hillebrandt, Nomoto, and Wolff (1983) calculated the collapse of the O+Ne+Mg core for case 2.2 and found that the shock wave generated at the bounce is strong enough to give rise to Type II supernova explosion which leaves a neutron star behind (see a review by Hillebrandt 1983). The final outcome of the collapse for case 2.4 must be the same because of similar presupernova structure. Thus 8–10 $M_\odot$ stars would produce a substantial fraction of Type II supernovae (SN II) and pulsars, which is consistent with the statistics by Tammann (1982) and Lyne (1982).

SN II from 8–10 $M_\odot$ progenitors would not contribute much to the heavy element synthesis since the ejecta would consist mostly of the material in the hydrogen-rich envelope which lies above the hydrogen-helium burning shells at $M_r = 1.375\ M_\odot$; most of the core material would form a neutron star (Hillebrandt, Nomoto, and Wolff 1983). Small abundance of heavy elements would be consistent with the

abundance of the Crab nebula (Davidson *et al.* 1982); in particular, small carbon abundance favors the core of $M_H^{(0)} = 2.2\ M_\odot$ as the Crab's progenitor (see Nomoto *et al.* 1982 for more detail).

On the other hand, 8–10 $M_\odot$ stars have been suggested to be possible progenitors of Type I supernovae (SN I) by Woosley, Weaver, and Taam (1980) and Weaver, Axelrod, and Woosley (1980). Weaver, Axelrod, and Woosley (1980) *assumed* that neon detonation is initiated in the O+Ne+Mg core of a 9 $M_\odot$ star and calculated the resultant light curve due to ^{56}Ni decay; this model assumed that a hydrogen-rich envelope is lost prior to the explosion.

Present investigation has shown that neon is never ignited for 8–10 $M_\odot$ stars with cores of $1.06\ M_\odot \leq M_{He} \leq 1.37\ M_\odot$ and that carbon shell burning proceeds nonexplosively (see § VII). In fact, the 9 $M_\odot$ star of Weaver, Axelrod, and Woosley (1980) has a core of $M_{He} < 1.37\ M_\odot$ at the dredge-up phase, and its evolution is similar to our core of $M_H^{(0)} = 2.2\ M_\odot$ (Nomoto *et al.* 1982). There remains a possible situation for thermonuclear explosion to occur in 8–10 $M_\odot$ stars; that is if the stars become helium stars before dredge-up. In this case, the growth rate of the C+O layer due to helium shell burning could be rapid enough to ignite a carbon shell flash as demonstrated by Nomoto (1982*c*) for a 2 $M_\odot$ helium star. Whether the flash grows into a detonation remains to be investigated.

A possible alternative scenario for 8–10 $M_\odot$ to be progenitors of SN I would be as follows: We adopt the evolutionary scenario described in § VIII*d*; i.e., 8–10 $M_\odot$ stars evolve to become red-giant–like helium stars by mass loss, and the O+Ne+Mg core collapses, triggered by electron captures. In this case, shock heating in the red-giant–like helium envelope could produce a SN I light curve near the peak (Lasher 1975). If at least $\sim 0.1\ M_\odot$ ^{56}Ni would be ejected from the collapsing core, ^{56}Ni decay could power the light curve tail (see Wheeler 1982 for a review). This model might be close to the model by Colgate, Petschek, and Kriese (1980). However, the iron peak elements ejected from the collapsing core could be too neutron-rich to contain enough ^{56}Ni although nucleosynthesis calculation has not yet been done.

IX. SUMMARY

The evolution of cores of stars near 10 $M_\odot$ is studied. Two cases with initial helium core mass of $M_H^{(0)} = 2.6\ M_\odot$ (case 2.6) and 2.4 $M_\odot$ (case 2.4) are discussed in this paper. (The case for $M_H^{(0)} = 2.2\ M_\odot$ will be discussed in Paper II.) The main conclusions are summarized as follows:

1. For these cores, carbon burning proceeds under non-degenerate conditions and leaves an O+Ne+Mg core.

2. For case 2.6, the mass of the O+Ne+Mg core (M_C) exceeds the critical mass for neon ignition (1.37 $M_\odot$) so that a strong off-center neon flash is ignited. The neon-oxygen shell burning layer moves inward.

3. For case 2.4, on the other hand, neon flash is not ignited because M_C ($= 1.34\ M_\odot$) is smaller than the critical mass for neon ignition. The O+Ne+Mg core becomes strongly degenerate.

4. The helium envelope for case 2.4 expands greatly when the C+O layer becomes thin in mass; this implies that the surface hydrogen convection zone starts to dredge up the helium layer. After dredge-up, evolution of the core would be the same as for the core of $M_H^{(0)} = 2.2\ M_\odot$ (Paper II; Nomoto 1983); the O+Ne+Mg core grows through the phase of hydrogen-helium double shell burning up to the onset of electron captures on ^{24}Mg and ^{20}Ne.

5. With regard to the nucleosynthesis, both cases have a common feature that the mass of the core interior to the helium burning shell is close to 1.4 $M_\odot$. Therefore they could not contribute much to the heavy element production in the Galaxy unless the supernova explosion is so energetic as to leave a neutron star of mass much smaller than 1.4 $M_\odot$.

6. Stars of 8–10 $M_\odot$ would give rise to Type II supernova explosions which leave neutron stars behind rather than Type I supernovae.

To summarize in terms of a helium core mass ($M_H^{(0)}$) and a corresponding main-sequence mass (M), a degenerate O+Ne+Mg core develops for $2\ M_\odot \lesssim M_H^{(0)} \lesssim 2.5\ M_\odot$ (i.e., $8\ M_\odot \lesssim M \lesssim 10\ M_\odot$), while $M_H^{(0)} > 2.5\ M_\odot$ ($M > 10\ M_\odot$) evolves beyond neon burning. The 8–10 $M_\odot$ stars would have a common final fate, i.e., the electron capture supernova which is triggered by the collapse of the O+Ne+Mg core due to electron captures (Miyaji *et al.* 1980).

The above scenario for 8–10 $M_\odot$ stars assumes that mass loss does not have a significant effect. If extensive mass loss occurs, or if the 8–10 $M_\odot$ star is in a close binary system, several variations in the final fate are possible:

1. If the mass loss rate is high enough during the helium burning phase, some 8–10 $M_\odot$ stars could become helium stars of 2–2.5 $M_\odot$ which have red-giant–like envelopes and would be observed as carbon stars. Such helium stars evolve into the electron capture supernovae.

2. If the mass loss during the double shell burnings is sufficiently rapid, stars in the lower end of the mass range of 8–10 $M_\odot$ would lose the envelope and become O+Ne+Mg white dwarfs instead of supernovae.

3. Stars of 8–10 $M_\odot$ in close binary systems would also leave O+Ne+Mg white dwarfs. These white dwarfs would grow and collapse into neutron stars by mass accretion.

The above summary suggests that evolution of stars in the mass range of 8–10 $M_\odot$ as well as slightly above 10 $M_\odot$ will have a variety of interesting outcomes and thus deserves further study.

It is a pleasure to thank Drs. W. M. Sparks, A. V. Sweigart, A. S. Endal, and D. Sugimoto for stimulating discussions, comments, and encouragement, J. C. Wheeler for the reading of the manuscript, and H. Nomoto for preparation of the manuscript and figures. This work has been supported in part by NRC-NASA Research Associateships in 1979–1981 and by the Grant-in-Aid for Scientific Research, Ministry of Education, Science, and Culture, Japan (58340023). The manuscript was completed during my stay at Max-Planck-Institut. I would like to thank Prof. R. Kippenhahn and Dr. W. Hillebrandt for their hospitality and discussions.

REFERENCES

Arnett, W. D. 1972*a*, *Ap. J.*, **176**, 681.
———. 1972*b*, *Ap. J.*, **176**, 699.
———. 1973, *Ap. J.*, **179**, 249.
———. 1974*a*, *Ap. J.*, **193**, 169.
———. 1974*b*, *Ap. J.*, **194**, 373.
———. 1982, *Ap. J.* (*Letters*), **263**, L55.
Barkat, Z. 1971, *Ap. J.*, **163**, 433.
Barkat, Z., Reiss, Y., and Rakavy, G. 1974, *Ap. J.* (*Letters*), **193**, L21.
Beaudet, G., Petrosian, V., and Salpeter, E. E. 1967, *Ap. J.*, **150**, 979.
Becker, S. A., and Iben, I., Jr. 1979, *Ap. J.*, **232**, 831.
———. 1980, *Ap. J.*, **237**, 111.
Boozer, A. H., Joss, P. C., and Salpeter, E. E. 1973, *Ap. J.*, **181**, 393.
Cazzola, P., De Zotti, G., and Saggion, A. 1971, *Phys. Rev.*, **D3**, 1722.
Chandrasekhar, S. 1939, *An Introduction to the Study of Stellar Structure* (Chicago: The University of Chicago Press).
Colgate, S. A., Petschek, A. G., and Kriese, J. T. 1980, *Ap. J.* (*Letters*), **237**, L81.
Colgate, S. A., and White, R. H. 1966, *Ap. J.*, **143**, 626.
Cottrell, P. L., and Lambert, D. L. 1982, *Ap. J.*, **261**, 595.
Cox, J. P., and Giuli, R. T. 1968, *Principles of Stellar Structure*, Vol. **1** (New York: Gordon and Breach), p. 281.
Cox, J. P., and Salpeter, E. E. 1964, *Ap. J.*, **140**, 485.
Davidson, K., *et al.* 1982, *Ap. J.*, **253**, 696.
Dicus, D. A. 1972, *Phys. Rev.*, **D6**, 941.
Dicus, D. A., Kolb, E. W., Schramm, D. N., and Tubbs, D. L. 1976, *Ap. J.*, **210**, 481.
Ebisuzaki, S., Hanawa, T., and Sugimoto, D. 1983, *Pub. Astr. Soc. Japan*, **35**, 17.
Endal, A. S. 1975*a*, *Ap. J.*, **195**, 187.
———. 1975*b*, *Ap. J.*, **197**, 405.
Ergma, E., and Vilhu, O. 1978, *Astr. Ap.*, **69**, 143.
Finzi, A., and Wolf, R. A. 1967, *Ap. J.*, **150**, 115.
Hayashi, C., Hoshi, R., and Sugimoto, D. 1962, *Prog. Theoret. Phys. Suppl.*, **22**, 1.
Hillebrandt, W. 1982*a*, in *Supernovae: A Survey of Current Research*, ed. M. J. Rees and R. J. Stoneham (Dordrecht: Reidel), p. 123.
———. 1982*b*, *Astr. Ap.*, **110**, L3.
———. 1983, preprint, review talk given at the XI Texas Symposium.
Hillebrandt, W., Nomoto, K., and Wolff, G. 1983, preprint.
Hoyle, F., and Fowler, W. A. 1960, *Ap. J.*, **132**, 565.
Iben, I., Jr. 1975, *Ap. J.*, **196**, 525.
Iben, I., Jr., and Truran, J. W. 1978, *Ap. J.*, **220**, 980.
Ikeuchi, S., Nakazawa, K., Murai, T., Hoshi, R., and Hayashi, C. 1972, *Prog. Theoret. Phys.*, **48**, 1890.
Joss, P. C., Katz, J. I., Malone, R. C., and Salpeter, E. E. 1973, *Ap. J.*, **181**, 409.
Kippenhahn, R. 1970, *Astr. Ap.*, **8**, 50.
Kumar, S. S. 1963, *Ap. J.*, **137**, 1121.
Kutter, G. S., and Savedoff, M. P. 1969, *Ap. J.*, **156**, 1021.
Lamb, S. A., Iben, I., Jr., and Howard, W. M. 1976, *Ap. J.*, **207**, 209.
Lasher, G. 1975, *Ap. J.*, **201**, 194.
Lyne, A. G. 1982, in *Supernovae: A Survey of Current Research*, ed. M. J. Rees and R. J. Stoneham (Dordrecht: Reidel), p. 405.
Miyaji, S., Nomoto, K., Yokoi, K., and Sugimoto, D. 1980, *Pub. Astr. Soc. Japan*, **32**, 303.
Murai, T., Sugimoto, D., Hoshi, R., and Hayashi, C. 1968, *Prog. Theoret. Phys.*, **39**, 619.
Nomoto, K. 1974, *Prog. Theoret. Phys.*, **52**, 453.
Nomoto, K. 1980*a*, in *Type I Supernovae*, ed. J. C. Wheeler (Austin: University of Texas), p. 164.
———. 1980*b*, *Space Sci. Rev.*, **27**, 563.
———. 1981, in *IAU Symposium 93, Fundamental Problems in the Theory of Stellar Evolution*, ed. D. Sugimoto, D. Q. Lamb, and D. N. Schramm (Dordrecht: Reidel), p. 295.
———. 1982*a*, *Ap. J.*, **253**, 798.
———. 1982*b*, *Ap. J.*, **257**, 780.
———. 1982*c*, in *Supernovae: A Survey of Current Research*, ed. M. J. Rees and R. J. Stoneham (Dordrecht: Reidel), p. 205.
———. 1982*d*, *Comments Ap.*, **9**, 301.
———. 1983, in *IAU Symposium 101, Supernova Remnants and Their X-Ray Emission*, ed. J. Danziger and P. Gorenstein (Dordrecht: Reidel), p. 139.
———. 1984, in preparation (Paper II).
Nomoto, K., Miyaji, S., Sugimoto, D., and Yokoi, K. 1979, in *IAU Colloquium 53, White Dwarfs and Variable Degenerate Stars*, ed. H. M. Van Horn and V. Weidemann (Rochester: University of Rochester), p. 56.
Nomoto, K., Sparks, W. M., Fesen, R. A., Gull, T. R., Miyaji, S., and Sugimoto, D. 1982, *Nature*, **299**, 803.
Nomoto, K., and Sugimoto, D. 1972, *Prog. Theoret. Phys.*, **48**, 46.
Paczyński, B. 1970, *Acta Astr.*, **20**, 47.
———. 1971, *Acta Astr.*, **21**, 271.
Rakavy, G., Shaviv, G., and Zinamon, Z. 1967, *Ap. J.*, **150**, 131.
Rees, M. J., and Stoneham, R. J., eds. 1982, *Supernovae: A Survey Of Current Research* (Dordrecht: Reidel).
Sparks, W. M., and Endal, A. S. 1980, *Ap. J.*, **237**, 130.
Sugimoto, D. 1971, *Prog. Theoret. Phys.*, **45**, 761.
Sugimoto, D., Eriguchi, Y., and Hachisu, I. 1981, *Prog. Theoret. Phys. Suppl.*, **70**, 154.
Sugimoto, D., and Miyaji, S. 1981, in *IAU Symposium 93, Fundamental Problems in the Theory of Stellar Evolution*, ed. D. Sugimoto, D. Q. Lamb, and D. N. Schramm (Dordrecht: Reidel), p. 191.
Sugimoto, D., and Nomoto, K. 1975, *Pub. Astr. Soc. Japan*, **27**, 197.
———. 1980, *Space Sci. Rev.*, **25**, 155.
Sugimoto, D., Nomoto, K., and Eriguchi, Y. 1981, *Prog. Theoret. Phys. Suppl.*, **70**, 115.
Tammann, G. A. 1982, in *Supernovae: A Survey of Current Research*, ed. M. J. Rees and R. J. Stoneham (Dordrecht: Reidel), p. 371.
Trimble, V. 1982, *Rev. Mod. Phys.*, **54**, 1183.
Unno, W. 1967, *Pub. Astr. Soc. Japan*, **19**, 140.
van den Heuvel, E. P. J. 1981, in *IAU Symposium 93, Fundamental Problems in the Theory of Stellar Evolution*, ed. D. Sugimoto, D. Q. Lamb, and D. N. Schramm (Dordrecht: Reidel), p. 155.
Weaver, T. A., Axelrod, T. S., and Woosley, S. E. 1980, in *Type I Supernovae*, ed. J. C. Wheeler (Austin: University of Texas), p. 113.
Weaver, T. A., Zimmerman, G. B., and Woosley, S. E. 1978, *Ap. J.*, **225**, 1021.
Webbink, R. F. 1979, in *IAU Colloquium 53, White Dwarfs and Variable Degenerate Stars*, ed. H. M. Van Horn and V. Weidemann (Rochester: University of Rochester), p. 426.
Weidemann, V. 1979, in *IAU Colloquium 53, White Dwarfs and Variable Degenerate Stars*, ed. H. M. Van Horn and V. Weidemann (Rochester: University of Rochester), p. 206.
Wheeler, J. C. 1981, *Rep. Progr. Phys.*, **44**, 85.
———. 1982, in *Supernovae: A Survey of Current Research*, ed. M. J. Rees and R. J. Stoneham (Dordrecht: Reidel), p. 167.
Woosley, S. E., Weaver, T. A., and Taam, R. E. 1980, in *Type I Supernovae*, ed. J. C. Wheeler (Austin: University of Texas), p. 96.

KEN'ICHI NOMOTO: Department of Earth Science and Astronomy, College of Arts and Sciences, University of Tokyo, Meguro-ku, Tokyo 153, Japan